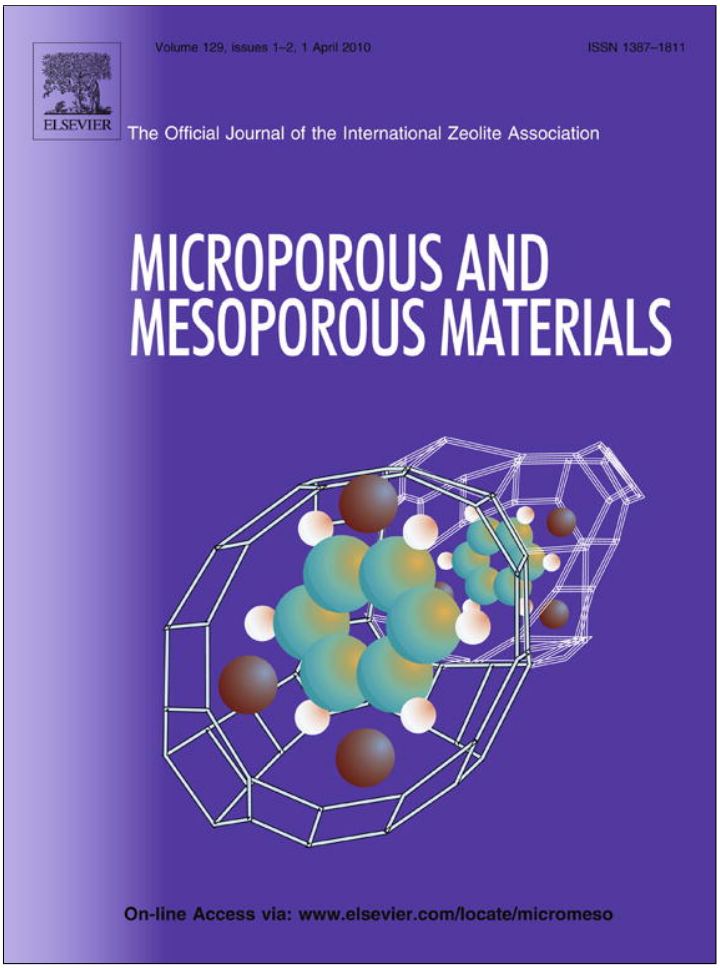

Microporous and Mesoporous Materials 129 (2010) 74–81

Contents lists available at ScienceDirect

Microporous and Mesoporous Materials

journal homepage: www.elsevier.com/locate/micromeso

# In–zeolites prepared by oxidative solid state ion exchange (OSSIE): Surface species and structural characterization

Juan M. Zamaro [a,*], Eduardo E. Miró [a], Alicia V. Boix [a], Angel Martínez-Hernández [b], Gustavo A. Fuentes [c]

[a] Instituto de Investigaciones en Catálisis y Petroquímica, INCAPE (FIQ, UNL, CONICET) Santiago del Estero 2829, 3000, Santa Fe, Argentina
[b] Facultad de Ciencias Químicas, Universidad Autónoma de Nuevo León, C.P. 66400, N.L., México
[c] Area de Ingeniería Química, Universidad A. Metropolitana – Iztapalapa, A.P. 55-534, 09340 D.F., México

ARTICLE INFO

*Article history:*
Received 21 July 2009
Received in revised form 21 August 2009
Accepted 29 August 2009
Available online 3 September 2009

*Keywords:*
Indium
Mordenite
ZSM5
Solid-state exchange

ABSTRACT

The characteristics of surface indium species and the transformations suffered by In–zeolite catalysts during the indium incorporation process by oxidative solid state ion exchange (OSSIE) are studied. This method causes a progressive dealumination of mordenite during the exchange process evidenced by $^{29}Si$ MAS NMR and $^{27}Al$ MAS NMR, producing a high proportion of octahedral aluminum that is further distorted at higher temperatures. However, ZSM5 is a much more stable framework for this exchange process. Exchanged indium $(InO)^+$ and highly-dispersed indium oxide species ($In_xO_y$) have the ability of adsorbing NO and further oxidizing it towards $NO_2$. Together with these dispersed species, a certain proportion of $In_2O_3$ crystals can be observed by XRD, which is higher for In–ZSM5. This zeolite presents a lower threshold dispersion capacity. Wider and asymmetric XPS In $3d_{5/2}$ signals indicate the presence of two surface indium species, one of them with a similar behavior to that of bulk oxide albeit not equal, and the other strongly interacting with the zeolite. The high temperature treatment does not modify the amount of surface indium species but changes their relative proportions. The quantity of highly dispersed species is increased on In–mordenite while the opposite occurs as regards on In–ZSM5. This latter zeolite is constituted by small, packed crystals with lower superficial acidic OH groups, which could originate a higher amount of voluminous polynuclear indium cations remaining on the zeolite crystal surface during impregnation, thus provoking the higher proportion of $In_2O_3$ outside channels after OSSIE. Structural modifications are also observed by FTIR being higher for mordenite, such as OH depletion by solid-state exchange, dehydroxilation and creation of extra-framework Al–OH species.



## 1. Introduction

Zeolites incorporated with indium have been studied in the last few years as catalysts for the selective catalytic reduction (SCR) of $NO_x$. In pioneering studies, Zhou et al. [1] and Kikuchi et al. [2] employed preparation methods for these catalysts based on thermal treatments in air atmosphere. By the same time, Beyer et al. [3] proposed a reductive method for In exchange (RSSIE). Several other methods for indium incorporation in zeolites were later proposed which resulted in a broad range of catalytic features for these solids, some of which were recently studied [4]. Of the above cited methods, the one most frequently used was the exchange by solid state reaction in reductant atmosphere (RSSIE) in which reductive and oxidative treatments were alternated to generate the indium active species [5,6]. Recently, Mihályi et al. [7] prepared an In/H–ZSM5 catalyst for $DeNO_x$ reactions from a mechanical mixture of $In_2O_3$ and H–ZSM5 heated in argon to 580 °C where indium suffered thermal auto-reduction and moved into exchange positions as $In^+$. Afterwards, $In^+$ was oxidized towards $(InO)^+$ in an oxygen flow.

On the other hand, active and selective catalysts have been obtained for the SCR of $NO_x$ with $CH_4$ in oxygen excess [8] using an indium exchange method that employs only oxidant atmospheres as used in [1,2]. The oxidative solid state ion exchange (OSSIE) method is based on the solid state reaction between indium oxide and the protons of the zeolite that takes place at high temperature under air atmosphere. Recently, this method has also been used for indium incorporation in catalytic zeolite films; highly active and selective structured catalysts were thus obtained for the $NO_x$ SCR reaction [9,10]. However, since this preparation route involves high temperature treatments in air and indium is first incorporated by impregnation, modifications could occur in the zeolite structure that finally determine the catalytic performance of these solids. The objective of this work is to characterize the physicochemical features of In–zeolites, such as framework integrity, type of indium species and their interaction with zeolite structure, on In–mordenite and In–ZSM5 catalysts prepared by the OSSIE method. For this

* Corresponding author.
*E-mail address:* zamaro@fiq.unl.edu.ar (J.M. Zamaro).

1387-1811/$ - see front matter © 2009 Elsevier Inc. All rights reserved.
doi:10.1016/j.micromeso.2009.08.035

reason we have carried out a detailed characterization of samples, employing Nuclear Magnetic Resonance Spectroscopy ($^{29}$Si MAS NMR and $^{27}$Al MAS NMR), X-ray Diffraction (XRD), X-ray Photoelectronic Spectroscopy (XPS), Scanning Electron Microscopy (SEM) and Fourier Transform Infrared Spectroscopy (FTIR).

## 2. Experimental

### 2.1. Materials and exchange procedure

The supports employed were the ammonium zeolites $NH_4$/mordenite (Zeolyst; Si/Al = 10) and $NH_4$/ZSM5 (Zeolyst; Si/Al = 15). The indium exchange was carried out in three steps: precursor impregnation, drying and high temperature treatments in air stream (synthetic air). The impregnation was performed stirring the zeolite powder with an excess of indium solution (0.5 g/l of In $(NO_3)_3$ Aldrich P.A.) while the solvent was evaporating. Once a paste slurry was obtained, it was dried at 120 °C overnight. Later, a calcination step in air was carried out increasing the temperature at 10 °C/min. For one set of samples the temperature was raised to 500 °C and maintained at this temperature for 12 h. For another set of samples, a second calcination step at 700 °C for 2 h was performed after the first treatment at 500 °C. In this way, different indium/zeolites treated at 500 °C and 700 °C were obtained with indium contents of 4 and 8 wt.% for both zeolites. Samples were labeled as follows: In(wt.%)/zeolite-treatment temperature (°C), for example In(4)/mor-500.

### 2.2. Characterization techniques

#### 2.2.1. Nuclear Magnetic Resonance of solids (MAS NMR)

$^{29}$Si HPDEC (high power decoupling) MAS NMR and $^{27}$Al MAS NMR spectra were acquired at 5 and 10 kHz, respectively, at room temperature with a Bruker Advance II instrument (300 MHz). Approximately 7000 scans for $^{29}$Si spectra were taken with acquisition times of about 0.015 s and 1000 scans for $^{27}$Al spectra were taken with acquisition times of 0.003 s. In this way, the populations of different silicon in zeolites as Si(4Si0Al), Si(3Si1Al), Si(2Si2Al) named $Q^4$, $Q^3$ and $Q^2$, respectively, were evaluated. The aluminum in octahedral ($Al^{oct}$) and tetrahedral ($Al^{tet}$) environments was also identified.

#### 2.2.2. X-ray Diffraction (XRD)

With this technique, the crystallinity of the zeolite phase and the presence of indium oxide clusters were determined. A Shimadzu XD-D1 instrument operated with Cu Kα radiation at 40 kV and 30 A was employed, with a scanning rate of 2 °/min between $2\theta = 5°$ and 65° which is the range where the most important signals of the zeolite and indium oxide can be found. The diffraction patterns obtained were compared to those of pure $NH_4$/ZSM5, $NH_4$/mordenite and $In_2O_3$ powders.

#### 2.2.3. X-ray Photoelectronic Spectroscopy (XPS)

XPS analyses were performed in a multi-technique system (SPECS) equipped with a dual Mg/Al X-ray source and a hemispherical PHOIBOS 150 analyzer operating in the fixed analyzer transmission (FAT) mode. The spectra were obtained with a pass energy of 30 eV; an Al Kα X-ray source was operated at 200 W and 12 kV. The working pressure in the analyzing chamber was less than $5 \times 10^{-9}$ mbar. Spectra were acquired in the In 3d, O 1s, C 1s, Si 2p, Si 2s and Al 2p regions. The Si 2p peak at 103.0 eV binding energy (BE) was taken as internal reference. The splitting of In $3d_{5/2}$–In $3d_{3/2}$ XPS signals was considered 7.6 eV for the signal processing. All the peaks were fitted by a Gaussian–Lorentzian component wave-form after an inelastic (Shirley-type) background had been subtracted in order to calculate the surface atomic ratio. The data processing and peaks deconvolution were performed using the Casa XPS software.

#### 2.2.4. Scanning Electron Microscopy (SEM)

Zeolite particles were analyzed by Scanning Electron Microscopy with a Jeol JSM-35C instrument operated at 23 kV acceleration voltages. Samples were first dispersed in water and then a drop of suspension was placed onto the sample holder. After that, the sample was dried and particles were coated with a thin layer of Au in order to improve the images.

#### 2.2.5. Fourier Transform Infrared Spectroscopy (FTIR)

Pelletized solids were prepared in a standardized way using an accessory to compress 100 mg of sample at equal pressures and times. The zeolite pellets were placed in an ISRI chamber with $CaF_2$ windows equipped with conducts for $N_2$ flow, cooling by water and heating by temperature-controlled cartridges. Afterwards, the zeolite was heated in $N_2$ flow at 350 °C and FTIR spectra were taken with a Bruker IFS 66 equipment. In this way, the OH stretching range (3000–4000 $cm^{-1}$) of the zeolites was measured. The interaction of NO on the sample surface was also studied by FTIR. For this purpose, the pellet was placed in a glass chamber with $CaF_2$ windows and evacuated in He flow at 350 °C for 4 h. It was then cooled to r.t. in He flow and immediately afterwards put in contact with a current of NO diluted in He (5000 ppm) for 20 min. Afterwards, NO was purged from the gas phase and the temperature was step-raised. At each temperature step, the FTIR spectrum of the pellet was taken with a Mattson Genesis II instrument.

## 3. Results and discussion

### 3.1. Nuclear Magnetic Resonance (MAS NMR) of solids

Fig. 1 shows the $^{29}$Si MAS NMR of fresh mordenite and the same solid treated at 500 °C and 700 °C. As can be observed, when the treatment temperature increases, the signals with lower chemical shift decrease in intensity and those with higher chemical shift increase, indicating a progressive change in the relative Si population

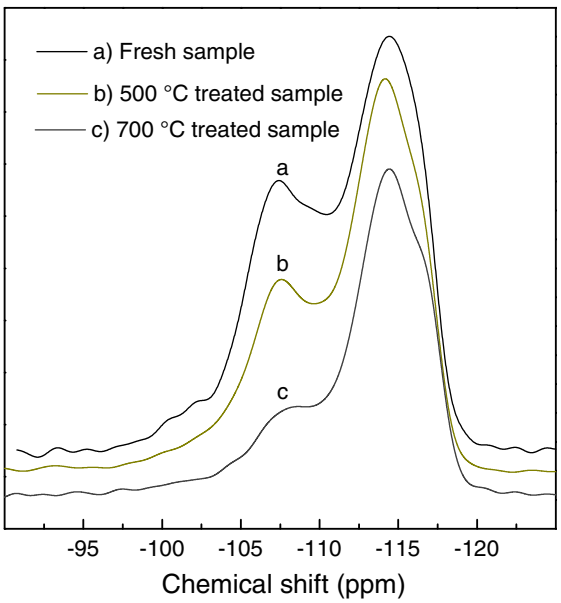


**Fig. 1.** $^{29}$Si NMR spectra of (a) fresh In(4)/mordenite and of the same solid treated in air at: (b) 500 °C and (c) 700 °C.

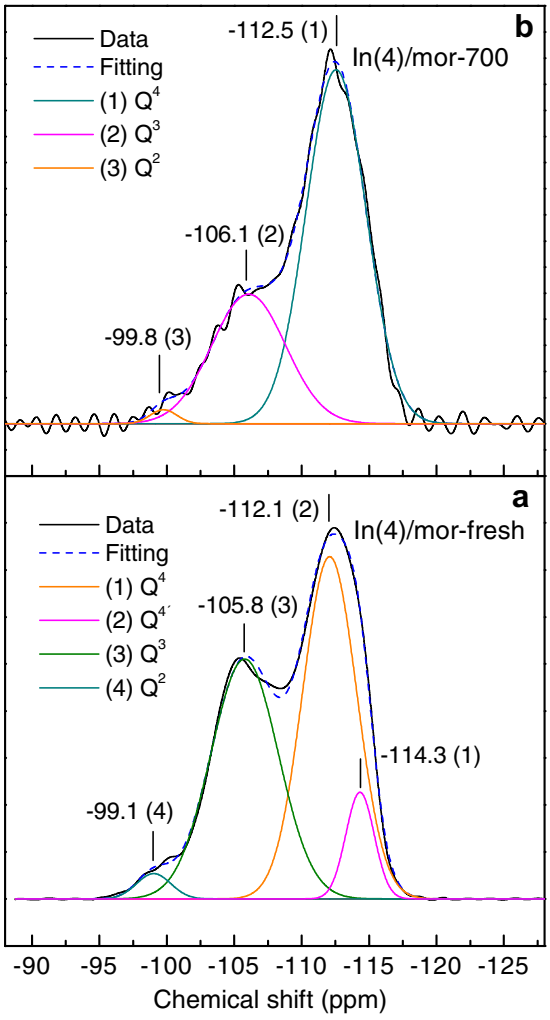


**Fig. 2.** $^{29}$Si NMR signals deconvolution for In(4)/mordenite. (a) Fitting of $^{29}$Si NMR signals for fresh In(4)/mordenite sample; (b) Fitting of $^{29}$Si NMR signals for In(4)/mordenite treated at 700 °C.

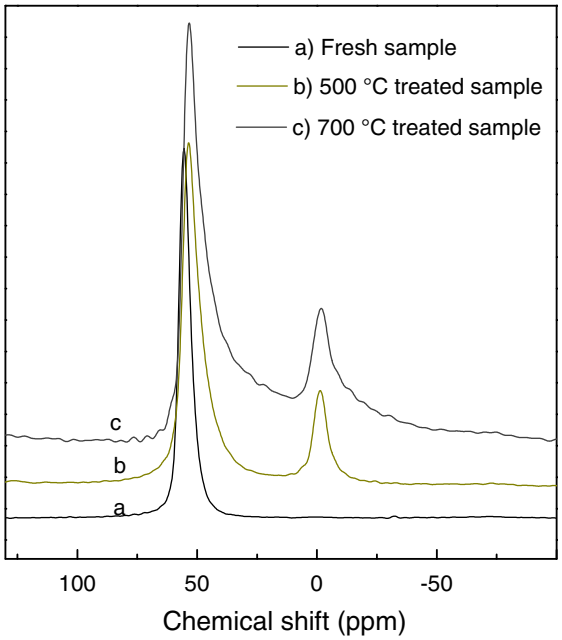


**Fig. 3.** $^{27}$Al NMR spectra of (a) fresh In(4)/mordenite and of the same solid treated in air at: (b) 500 °C and (c) 700 °C.

due to a dealumination process. The $^{29}$Si NMR chemical shift signal positions agree with those reported for this zeolite [11], located at −113 ppm ($SiQ^4$), −106 ppm ($SiQ^3$) and −100 ppm ($SiQ^2$). The splitting of the $SiQ^4$ broad signal for dealuminated mordenite reflects silicon atoms in crystallographic non-equivalent T sites, as previously reported [12]. The deconvolution of the $^{29}$Si NMR signals for the In(4)/mor samples (Fig. 2) allowed us to calculate the proportions of $SiQ^2$, $SiQ^3$ and $SiQ^4$, as shown in Table 1. The amount of $SiQ^2$ and $SiQ^3$ (surrounded by a higher number of Al atoms) decreases when the temperature increases. The dealumination is verified by $^{27}$Al MAS NMR (Fig. 3); a significant proportion of Al in octahedral coordination or extra-framework Al (at 0 ppm) can be observed in the sample treated at 500 °C. The main neighbouring signal located at 54 ppm is from the mordenite Al framework, tetrahedrically coordinated as reported elsewhere [13]. It can also be observed that the treatment at 700 °C provokes a higher distortion of the zeolitic structure, evidenced by the deformation of the Al environment, both for octahedral and tetrahedral coordination, as suggested by the tail of the $^{27}$Al MAS NMR signal. In this sample treated at 700 °C, the possible presence of other minor phases of Al species such as polymeric Al, $Al_2O_3$ or amorphous silica cannot be ruled out because the low symmetry environment of these species could be responsible for a slight broadening at the base of the $^{27}$Al NMR signals (Fig. 3) under the narrow Al peaks [13].

Table 1 shows that for the In–ZSM5 samples a slight modification of the $SiQ^3$ and $SiQ^4$ proportions with the thermal treatments takes place. Silicon peaks at −115, −112 and −105 ppm are observed (not shown) in agreement with lines attributed to the $Q^4$, $Q^{4\prime}$ and $Q^3$ units of the ZSM5 framework [14]. The small change of the NMR signals accounts for the higher thermal stability of this zeolite even with treatments at 700 °C. However, the $^{27}$Al MAS NMR spectra show a small peak of octahedral Al indicating a slight initial dealumination in the fresh sample, which slightly increases when treated at 700 °C (Table 1).

### 3.2. X-ray Photoelectronic Spectroscopy (XPS)

Framework modifications observed by NMR were produced simultaneously to changes in surface indium species. In all the samples studied in this work, widening and asymmetries were observed in the $3d_{5/2}$ XPS signals. Moreover, the fitting of the In $3d_{5/2}$ spectra could only be done by considering two signals. This indicates the presence of two types of surface species. The same

**Table 1**
Proportions of the different silicon and aluminum poblations for fresh and OSSIE treated indium/zeolites, determined by $^{29}$Si MAS NMR and $^{27}$Al MAS NMR signals deconvolution.

| Signal | In(4)/mor-700 | In(4)/mor-fresh | In(4)/ZSM5-700 | In(4)/ZSM5-fresh |
|---|---|---|---|---|
| $SiQ^4$ | 68.0[a] | 55.8 | 84.1 | 88.2 |
| $SiQ^3$ | 30.8 | 42.0 | 16.0 | 11.8 |
| $SiQ^2$ | 1.2 | 2.2 | – | – |
| $Al^{tet}/Al^{oct}$ | 4.3 | ∞ | 11.8 | 17.6 |

[a] Corresponds to $Q^4 + Q^{4\prime}$ from Fig. 2.

**Table 2**
XPS binding energies and surface elemental ratios determined by signal processing for indium zeolites obtained by OSSIE.

| Signal ratios | In(4)/mor-500 | In(4)/mor-700 | In(8)/mor-500 | In(8)/mor-700 | In(4)/ZSM5-500 | In(4)/ZSM5-700 | In(8)/ZSM5-500 | In(8)/ZSM5-700 |
|---|---|---|---|---|---|---|---|---|
| In $3d_{5/2}$[a]/In $3d_{5/2}$[b] | 0.57 | 0.74 | 0.73 | 0.82 | 0.41 | 0.30 | 0.31 | 0.20 |
| In $3d_{5/2}$[c]/Si 2p | 0.023 | 0.021 | 0.038 | 0.034 | 0.021 | 0.023 | 0.047 | 0.043 |
| Si 2p/Al 2p | 13.87 | 13.20 | 12.2 | 11.8 | 18.5 | 19.1 | 18.0 | 19.9 |
| BE (eV)[d] | | | | | | | | |
| In $3d_{5/2}$[a] | 446.3 | 446.4 | 446.3 | 446.2 | 445.5 | 445.7 | 445.7 | 445.9 |
| In $3d5_{/2}$[b] | 445.0 | 444.8 | 444.8 | 444.7 | 443.9 | 443.9 | 444.0 | 444.2 |
| Al 2p | 73.9 | 74.6 | 73.9 | 74.1 | 74.1 | 74.1 | 74.1 | 74.4 |

Nominal Si/Al of $NH_4$/mordenite = 10; Si/Al by XPS for H/mor-700 = 12.4.
Nominal Si/Al of $NH_4$/ZSM5 = 15; Si/Al by XPS for H–ZSM5-700 = 19.3.
Measured XPS BE for $In_2O_3$ = 443.2 eV.
[a] High binding energy.
[b] Low binding energy.
[c] In $3d_{5/2}$[a] + In $3d_{5/2}$[b].
[d] The binding energies (BE) were referred to Si 2p = 103 eV.

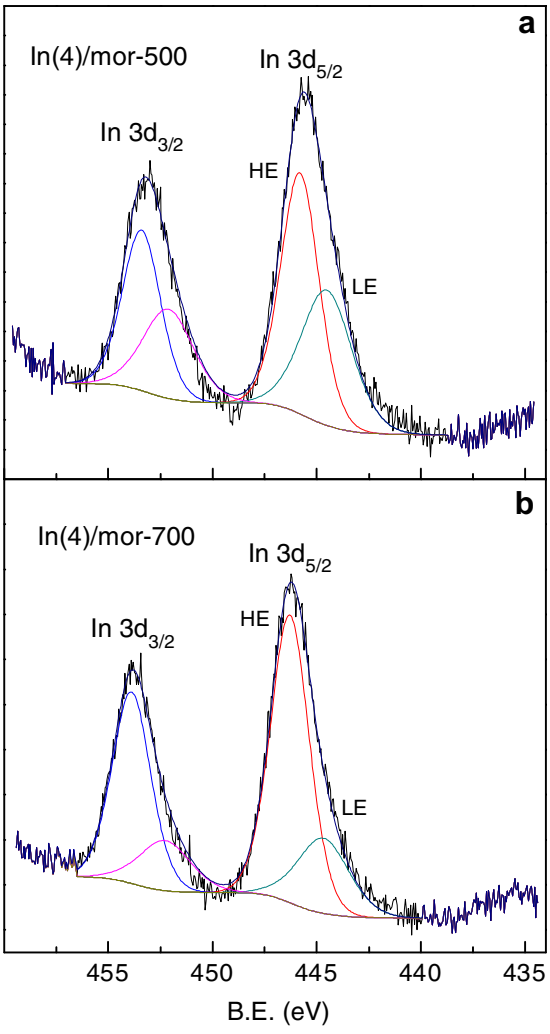


**Fig. 4.** In 3d XPS signals processed for In(4)/mordenite obtained by OSSIE at 500 °C and 700 °C (HE: species with higher binding energy; LE: species with lower binding energy).

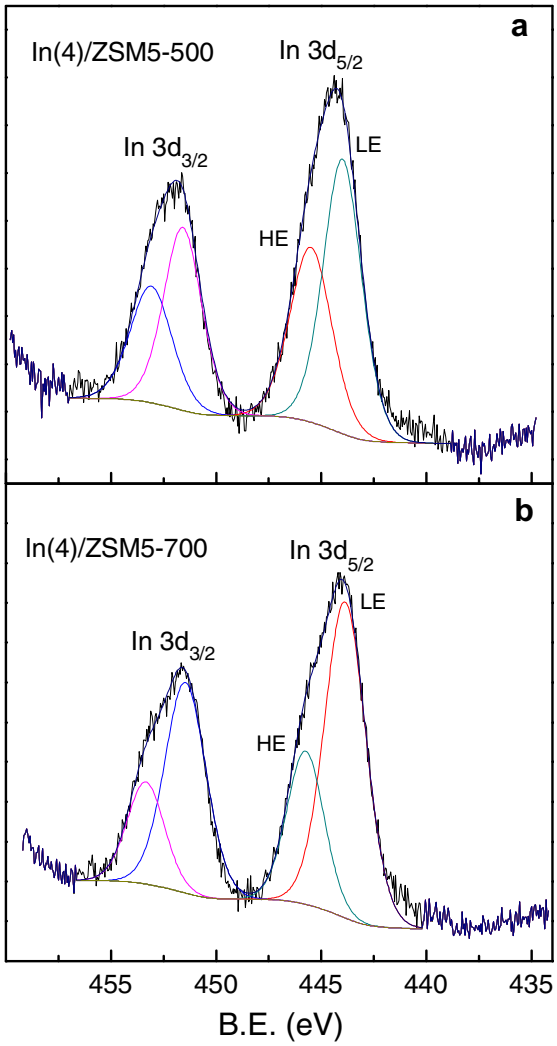


**Fig. 5.** In 3d XPS signals processed for In(4)/ZSM5 obtained by OSSIE at 500 °C and 700 °C (HE: species with higher binding energy; LE: species with lower binding energy).

characteristic was reported for temperature-treated $In_2O_3$/ZSM5 physically mixed solids [15] and for In–zeolites prepared by the RSSIE method [16]. One In $3d_{5/2}$ XPS signal (LE) was located at 444 eV for mordenite and 445 eV for ZSM5, associated with species with a structure similar to, but slightly higher than, that of the bulk oxide, because the bulk $In_2O_3$ presented a $3d_{5/2}$ signal at 443.2 eV (Table 2). The other In $3d_{5/2}$ XPS signal (HE) was found at higher binding energy (around 446 eV), associated with species that interact strongly with the zeolite (exchanged $(InO)^+$ and/or $In_xO_y$ species). This high interaction could only be achieved by indium species in zeolite intrapore (near the pore mouth) at exchangeable positions, as observed for other cations exchanged in zeolites [16].

Fig. 4 shows the XPS spectra of In(4)/mor treated at different temperatures, indicating that a change in the distribution of surface indium species has taken place. A similar behavior is observed when the In loading increases. However, the signal deconvolution and integration indicates that the In/Si ratio remains unchanged. The XPS results are summarized in Table 2.

In the In–ZSM5 samples (Fig. 5), the coexistence of two kinds of indium surface species is also observed. Similarly to In/mor, in the sample treated at 500 °C (Fig. 7a) an amount of species that interact with the zeolite (HE) is present. However, the treatment at 700 °C gives place to a change in the species distribution for In–ZSM5 which is different from that observed for In–mordenite samples. It can be seen that while the low energy (LE) In 3d signal increases, the signal corresponding to high interaction (HE) indium species decreases (see Table 2). Since the In/Si ratio remains constant (Table 2), the said effect should be originated in an interconversion of indium species near the zeolite surface and not in the diffusion of these species inside the zeolite crystals. The lesser amount of acidic external OH groups in ZSM5 could contribute to the lower proportion of superficially dispersed indium species after the high temperature treatment. This point will be taken up in the next subsections.

On the other hand, the XPS results indicate that the Si/Al ratios of the samples are higher with respect to the theoretical bulk values (see Table 2, footnote). In the case of In–mordenites, the Si/Al ratios are also higher than the XPS measured ratios for the H-mordenite treated at 700 °C (see Table 2, footnote), while for In–ZSM5 they are similar to those of H–ZSM5. The mordenite behaviour could be related to differences in the dealumination process.

### 3.3. X-ray Diffraction (XRD)

To investigate the crystalline indium phases and the changes on the crystalline structure of zeolites produced by the OSSIE treatment, XRD measurements were carried out. The crystalline $In_2O_3$ presents the main diffraction peaks at $2\theta = 30.64°$, 35.48°, 51.16° and 60.8° (Fig. 6). For In(4)/mor-700 the peaks corresponding to indium oxide phases are not observed, but for In(8)/mor-700 the main peaks of the $In_2O_3$ oxide become detectable (Fig. 6). On the other hand, when ZSM5 is the support, the sample with the lower In loading (4 wt.%) presents the characteristic $In_2O_3$ peaks (Fig. 7), although in other studies the indium oxide has not been observed in samples with less than 5 wt.% [1]. The dispersion threshold of indium is reached with a lower loading on ZSM5. Accordingly, for the In(8)/ZSM5 sample, the intensity of $In_2O_3$ peaks increases (Fig. 7).

The XRD patterns also show the peaks corresponding to the zeolitic structures. For mordenite sample, an important reduction of peaks at low angles (below 10°) can be seen, which could be originated by the partial collapse of the mordenite structure, in agreement with the previous NMR characterization results. However, in

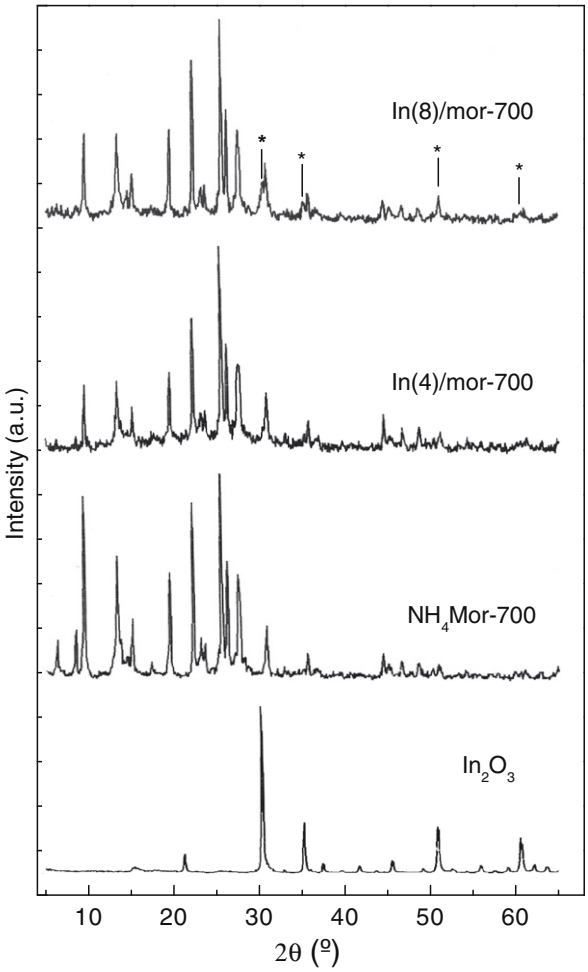


**Fig. 6.** X-ray diffraction patterns of ammonium and indium/mordenite samples with 4 wt.% and 8 wt.% indium loading. The figure shows In–mordenite samples treated by OSSIE at 700 °C. $In_2O_3$ diffractogram is shown for comparison (asterisk denotes $In_2O_3$ signals).

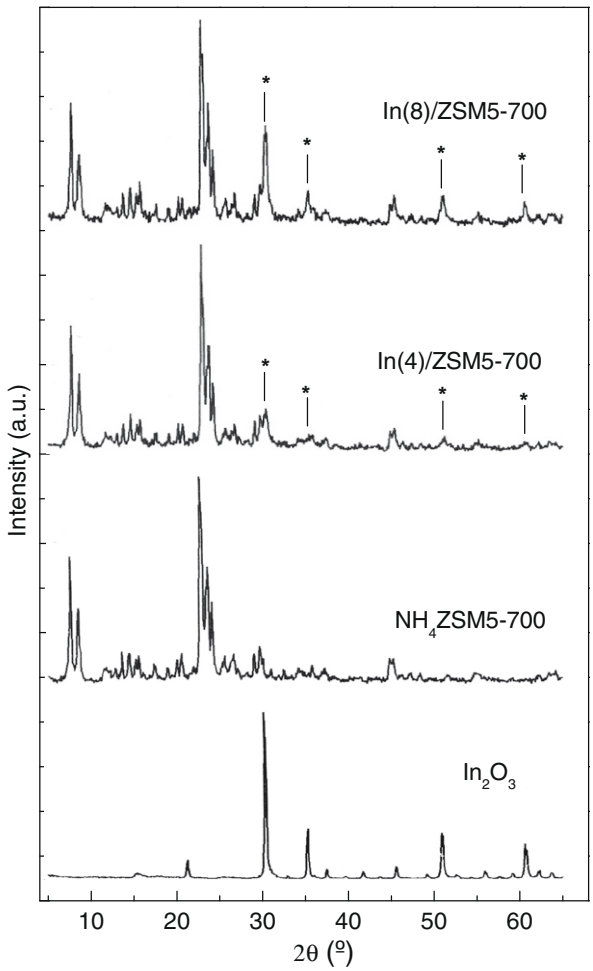


**Fig. 7.** X-ray diffraction patterns of ammonium and indium/ZSM5 samples with 4%wt and 8 wt.% indium loading. The figure shows In–ZSM5 samples treated by OSSIE at 700 °C. $In_2O_3$ diffractogram is shown for comparison (asterisk denotes $In_2O_3$ signals).

the case of In–ZSM5 this effect is not observed indicating the better thermal stability of this zeolite.

It should be mentioned that the XRD of these indium/zeolites treated at 500 °C showed similar characteristics to those of the samples treated at 700 °C (not shown). Only a lower depletion of low angle signals of mordenite framework was observed, supporting the assumption that the disappearance of these signals is due to a partial structure collapse.

### 3.4. Scanning Electron Microscopy (SEM)

The formation of different proportions of indium species in the zeolites as showed in the above characterizations, could be influenced by the characteristic of zeolite particles. This is a feature not so frequently taken into account which could have an impact on the properties of In–zeolites prepared by wet methods. Ogura et al. have studied the particle size effect of ZSM5 in the indium sites creation for In–ZSM5 catalysts [17], finding that particle size alters the proportion of indium species at the external surface. The FTIR results presented in next section show that the amount of acidic OH groups in $NH_4$/mordenite treated at 500 °C (H–mordenite) is higher than for H–ZSM5. On the other hand, the OH groups in zeolites could exist both outside and inside the crystals, the amount of external OH groups being dependent on the external specific area of the crystal surface [18]. Previously, we determined that ZSM5 particles have a particle size distribution with $d^{0.5}$ = 3.9 μm and mordenite particles have a $d^{0.5}$ = 2.6 μm with a wider, and shifted to smaller, size particle volume distribution [9]. The SEM pictures (Fig. 8) show that ZSM5 is constituted by densely packed small crystals (0.2 μm) forming nearly spherical aggregates. Instead, mordenite particles (Fig. 9) are constituted by a higher proportion of isolated crystals and some aggregated crystals forming low packed and less spherical particles. These structural characteristics of zeolite crystals may affect the behavior of In species during the impregnation and drying steps. During these processes, polynuclear cations $In[(OH)_2In]_n^{3+n}$ could be formed and deposited on the external surface of the crystals [8]. The higher volume of the ZSM5 particles constituted by small and packed crystals with a lower superficial acidic OH groups could originate a higher amount of the voluminous polynuclear indium cations remaining on the zeolite crystal surface. After the high temperature treatment of this solid (i.e. 700 °C), a great proportion of $In_2O_3$ crystals was formed onto the crystal surface thus explaining the XPS observations for this In–zeolite. The opposite XPS behavior determined for In–mordenite (diminution of surface $In_2O_3$ with 700 °C treatment) could be explained by the low packed characteristics of these crystals, which have a higher amount of superficial acidic OH groups. This zeolite also has a bigger one-dimensional channel network. All these features could allow a higher quantity of highly-dispersed indium oxide species (as $(InO)^+$ and dispersed $In_xO_y$) at the crystal surface and intrapore after the 700 °C treatment.

### 3.5. Fourier Transform Infrared Spectroscopy (FTIR)

As previously shown, the thermal treatment performed in zeolites for the indium exchange, generated structural changes and different indium species. As the exchange is produced by reaction of indium with protonic zeolite sites, we acquired the FTIR spectra of the solids in the region of the zeolite OH groups. Fig. 10 shows that for the $NH_4$/zeolite samples treated at 500 °C, sharp signals from OH vibrations at 3600 $cm^{-1}$ are present, indicating the total development of H/zeolite forms. Treatment at 700 °C causes a depletion of the 3600 $cm^{-1}$ signal for both In–zeolites, being higher for mordenite, in agreement with the decrease of acidic zeolite OH due to the solid state reaction with $In_2O_3$ [15] according to $In_2O_3 + H^+Zeolite^- \rightarrow 2(InO)^+Zeolite^- + H_2O$. However, in the ammonium treated samples this signal also decreases, suggesting that a thermal dehydroxilation could be simultaneously produced for the indium treated samples. For $NH_4$/mor-500, the 3600 $cm^{-1}$ band has a shoulder at lower frequencies (3570 $cm^{-1}$) indicating the presence of two different acidic OH (Fig. 10a). For $NH_4$/ZSM5-500, the 3600 $cm^{-1}$ band is symmetric in agreement with only one environment of acidic OH groups (Fig. 10b).

A signal at 3650 $cm^{-1}$ is also observed for both zeolites after treatment at 500 °C, which increases after treatment at 700 °C. It can be assigned to $Al(OH)^{2+}$ and $Al(OH)_2^+$ species originated due to migration and hydration of the aluminum of the zeolite framework [19]. The increase of this signal after the 700 °C treatment for H–mordenite (Fig. 10a) implies that it suffers dealumination in air

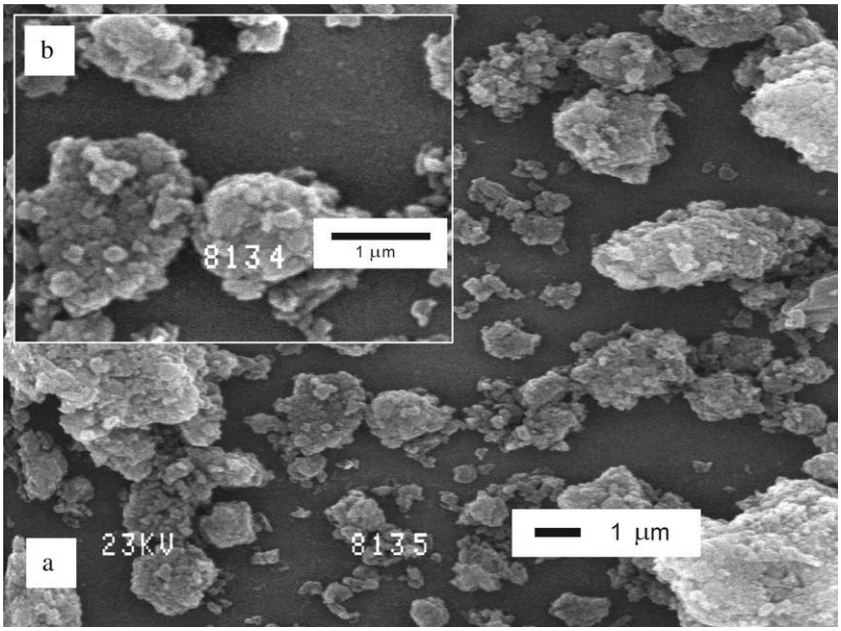


**Fig. 8.** SEM images of ZSM5 particles. (a) General view of the packed aggregates of ZSM5; (b) close view showing a detail of the aggregates, composed of small ZSM5 crystals.

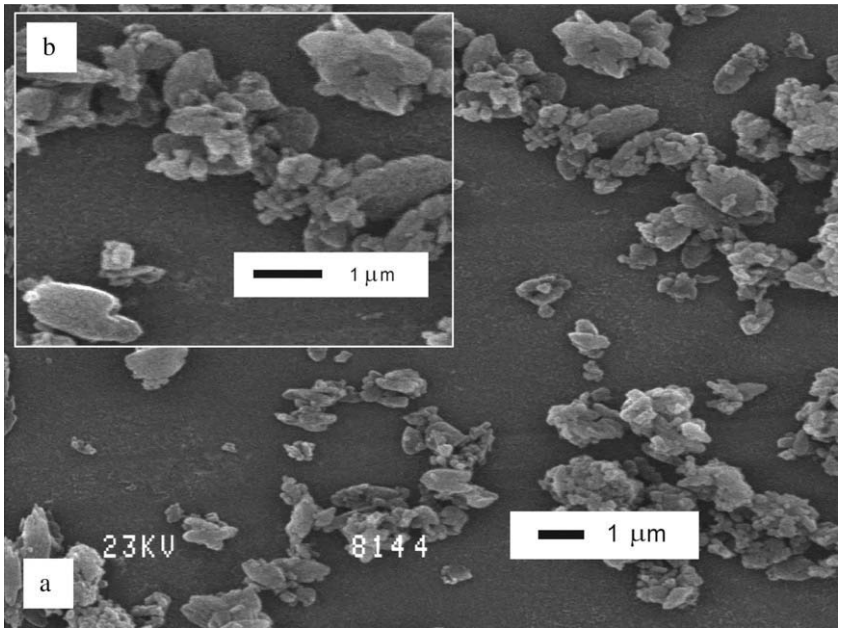


**Fig. 9.** SEM images of mordenite particles. (a) General view of the mordenite particles composed by isolated and low packed aggregates; (b) close view of an aggregate, showing the less packed structure.

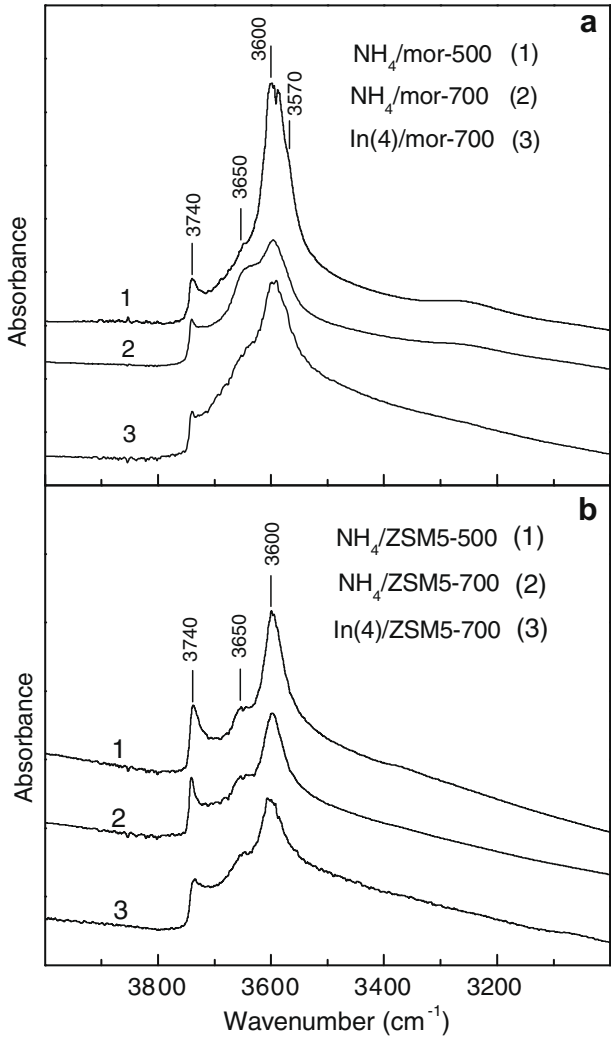


**Fig. 10.** FTIR spectra of $NH_4$ and In–zeolites pellets taken at 350 °C with $N_2$ flow. (a) FTIR spectra of mordenite samples; (b) FTIR spectra of ZSM5 samples.

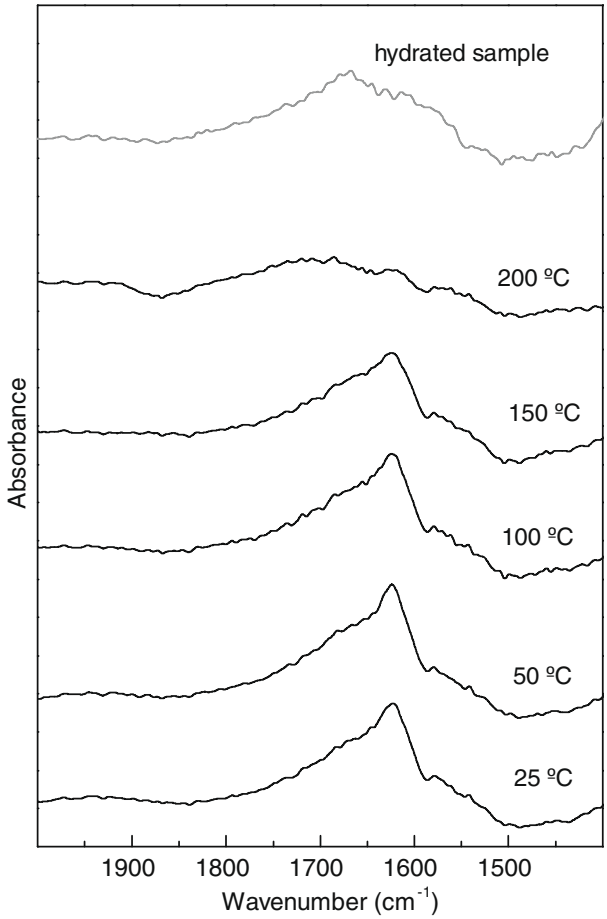


**Fig. 11.** FTIR spectra of dehydrated In(4)/mordenite sample treated by OSSIE at 700 °C, pelletized and treated with NO. The spectra were taken after gas phase evacuation at different temperatures.

stream at 500 °C for 12 h, which is increased after the 2-h 700 °C additional treatment, in agreement with structural modifications

detected by the NMR studies reported above. The decrease in the relative intensity of the 3650 $cm^{-1}$ band for the In(4)/mor-700 sample could be originated by interaction between indium species and extralattice Al–OH species, as proposed for indium ion-exchanged samples [5]. For the $NH_4$/ZSM5 treated samples (Fig. 10b), the 3650 $cm^{-1}$ signal is present after the 500 °C treatment but smaller changes are observed after the 700 °C treatments, if compared to mordenite, in agreement with the small NMR changes for octahedral aluminum.

The indium exchange process by the OSSIE method in zeolites treated at 700 °C was also reflected in the catalytic performance of these solids. The samples evaluated in the $NO_x$ SCR with $CH_4$ and 2% $O_2$ at 15,000 $h^{-1}$ (1000 ppm NO, 1000 ppm $CH_4$) showed a maximum $NO_x$ conversion of 44% at 370 °C for In(4)/mordenite, while In(4)/ZSM5 reached 72% at 500 °C, in spite of the lower amount of dispersed indium species present in the latter. A thorough catalytic evaluation of these samples is currently in progress [20].

### 3.6. Fourier Transform Infrared Spectroscopy (FTIR) of adsorbed NO

The dispersed indium species produced during the OSSIE method shown by the FTIR and XPS results were further confirmed by NO-FTIR experiments. In previous studies, we found a characteristic $NO_2$ evolution in NO-temperature programmed experiments of In–zeolites [10], associated with a NO oxidation by the dispersed indium species followed by a $NO_2$ desorption above 200 °C. FTIR experiments were carried out using pellets of In/mor treated in NO atmosphere and evacuated at different temperatures (Fig. 11). It can be observed that after evacuation at low temperatures, the only $NO_x$ signal detected on the solid is the one located at 1628 $cm^{-1}$, which corresponds to the stretching of $NO_2$ bondings. The signal corresponding to the OH bonding of water is also in this zone, but with lower definition and shifted to higher wave numbers (see hydrated sample). The adsorbed $NO_2$ signal becomes weaker after evacuation at 200 °C, which is consistent with the depletion of $NO_2$ observed in NO-TPD experiments on similar In–zeolite samples [10].

## 4. Conclusions

By NMR, it was determined that the indium exchange process to obtain In–zeolite catalysts by the OSSIE method causes changes in the zeolite structure even at 500 °C and especially in mordenite. A progressive dealumination occurs when increasing temperature, changing the relative amounts of extra-framework Al together with a distortion of the zeolitic structure. ZSM5 is a more stable support for the OSSIE method. In samples with 4 wt.% indium, crystals of $In_2O_3$ are observed for ZSM5; the threshold limit of indium dispersion is higher with mordenite. Dispersed indium species in this zeolite can oxidize NO to $NO_2$, which desorbs at low temperatures. These dispersed indium species are responsible for the catalytic activity of these solids in the SCR of $NO_x$. The OSSIE treatment originates different indium species on the surface, as determined by XPS measurements. The surface indium content is similar in both zeolites but the proportions of species are different. For In–mordenite, ($InO^+$, $In_xO_y$) species are preferentially formed and they increase with the temperature treatment, whereas for ZSM5 the contrary occurs. This could be attributed to a larger amount of strong acidic OH surface sites in the smaller and less packed mordenite crystals, which would favor surface interactions with indium species.

Structural changes also impact on the OH zeolite groups. FTIR characterization indicates that extra-framework AlOH type species are formed after treatment at 500 °C. At higher temperatures, the decrease of the amount of acidic OH is produced due to both the solid-state exchange and thermal dehydroxilation. These effects are more pronounced in mordenite samples.

## Acknowledgements

The authors are grateful for the financial support received from Project CIAM, Universidad Nacional del Litoral, and CONICET from Argentina; Universidad Autónoma Metropolitana and CONACYT from Mexico. Thanks are also given to ANPCyT for Grant PME 8-2003 to finance the purchase of the UHV multi-analysis system, to Elsa Grimaldi for the English language editing, and to Drs. Marco Antonio Vera and Atilano Gutiérrez from UAMI, Mexico for their technical assistance in the NMR spectra acquisition.

## References

[1] X. Zhou, T. Zhang, Z. Xu, L. Lin, Catal. Lett. 40 (1996) 35.
[2] E. Kikuchi, M. Ogura, I. Terasaki, Y. Goto, J. Catal. 161 (1996) 465.
[3] H.K. Beyer, R.M. Mihályi, Ch. Minchev, Y. Neinska, V. Kanazirev, Micropor. Mater. 7 (1996) 333.
[4] C. Schmidt, T. Sowade, E. Lffler, A. Birkner, W. Grünert, J. Phys. Chem. B 106 (16) (2002) 4085.
[5] T. Sowade, C. Schmidt, F.W. Schütze, H. Berndt, W. Grünert, J. Catal. 214 (2003) 100.
[6] H. Solt, F. Lónyi, R.M. Mihályi, J. Valyon, L.B. Gutiérrez, E.E. Miró, J. Phys. Chem. 112 (2008) 19423.
[7] R.M. Mihályi, Z. Schay, Á. Szegedi, Catal. Today 143 (2009) 253.
[8] E.E. Miró, L. Gutiérrez, J.M. Ramallo-López, F.G. Requejo, J. Catal. 188 (1999) 375.
[9] J.M. Zamaro, María A. Ulla, Eduardo E. Miró, Chem. Eng. J. 106 (2005) 25.
[10] J.M. Zamaro, María A. Ulla, Eduardo E. Miró, Appl. Catal. A: Gen. 314 (2006) 101.
[11] W. Schwieger, D. Heidemann, K.H. Bergk, Rev. Chim. Miner. 22 (1985) 639.
[12] W.M. Meier, H.J. Moeck, J. Solid State Chem. 27 (1979) 349.
[13] M. Lezcano, A. Ribotta, E. Miró, E. Lombardo, J. Petunchi, C. Moreaux, J.M. Dereppe, J. Catal. 168 (1997) 511.
[14] J.B. Nagy, J.P. Gilson, E.G. Derouane, J. Chem. Soc., Chem. Commun. (1981) 1129.
[15] M. Ogura, N. Aratani, E. Kikuchi, Stud. Surf. Sci. Catal. (1997) v.105.
[16] C. Schmidt, T. Sowade, F.W. Schütze, M. Ritcher, H. Berndt, W. Grünert, in: Proceedings of the 13th International Zeolite Conference, Montpellier, France, 2001.
[17] M. Ogura, T. Ohsaki, E. Kikuchi, Micropor. Mesopor. Mater. 21 (1998) 533.
[18] S.B. Pu, T. Inui, Zeolites 19 (1997) 452.
[19] A. Zecchina, S. Bordiga, G. Spoto, D. Scarano, G. Petrini, G. Leofanti, M. Padovan, C. Otero Areán, J. Chem. Soc., Faraday Trans. 88 (1992) 2959.
[20] J.M. Zamaro et al., J. Mol. Catal. A: Chem. (2009), submitted for publication.